Research Square

Preprints are preliminary reports that have not undergone peer review.
They should not be considered conclusive, used to inform clinical practice,
or referenced by the media as validated information.

An Efficient Virtual Statistical Energy Analysis Method for Cylindrical Periodic Structures Based on the Group Theory and Wittrick-Williams Algorithm

Haikuan Dong
Dalian University of Technology
Bowen Yan
China Aerodynamics Research and Development Center
Ziyi Liu
Dalian University of Technology
Zhengjie Li
China Aerodynamics Research and Development Center
Qiang Gao
qgao@dlut.edu.cn

Dalian University of Technology

Research Article

Keywords: Virtual Statistical Energy Analysis, Modal density, Cylindrical periodic structure, Group theory, Wittrick-Williams algorithm

Posted Date: November 12th, 2026

DOI: https://doi.org/10.21203/rs.3.rs-11466385/v1

License: This work is licensed under a Creative Commons Attribution 4.0 International License.
Read Full License

Additional Declarations: No competing interests reported.

An Efficient Virtual Statistical Energy Analysis Method for Cylindrical Periodic Structures Based on the Group Theory and Wittrick-Williams Algorithm

Haikuan Dong[1], Bowen Yan[2], Ziyi Liu[1], Zhengjie Li[2], Qiang Gao[1,*]

[1]*State Key Laboratory of Structural Analysis, Optimization and CAE Software for Industrial Equipment, Department of Engineering Mechanics, School of Mechanics and Aerospace Engineering, Dalian University of Technology, Dalian 116024, P.R. China*

[2]*High Speed Aerodynamic Institute, China Aerodynamics Research and Development Center, Mianyang 621000, China*

Email: 18345152792@163.com, 2747193795@qq.com, lzy98@mail.dlut.edu.cn, afeu_lzj@163.com, qgao@dlut.edu.cn

[*]*Corresponding author: E-mail address: qgao@dlut.edu.cn*

October, 2026

Abstract: This paper proposes an efficient Virtual Statistical Energy Analysis (VSEA) method for cylindrical periodic structures. The application of VSEA to such complex structures is generally limited by two computational bottlenecks: modal density calculation for determining valid analysis frequency bands, and global modal analysis required for SEA parameter calculation. To address these issues, the cylindrical periodic structure is first circumferentially decoupled based on group theory, transforming the coupled eigenvalue problem into a set of independent subproblems. On this basis, modal density is efficiently calculated using the Wittrick-Williams (W-W) algorithm, and an efficient method combining the W-W algorithm with the bisection method is developed to obtain the natural frequencies and mode shapes required for SEA parameter calculation. Finally, the Power Injection Method (PIM) is employed to determine the SEA parameters and calculate the subsystem energy responses. Numerical examples show that the proposed method achieves high accuracy and significantly improves computational efficiency compared with commercial software.

Keywords: Virtual Statistical Energy Analysis; Modal density; Cylindrical periodic structure; Group theory; Wittrick-Williams algorithm

1. Introduction

Cylindrical periodic structures are widely used in aerospace, automotive, and marine engineering due to their excellent load-bearing capacity, lightweight characteristics, and high structural efficiency (Qu et al., 2013; Guo et al., 2025; Ashari

and Stephen, 2026; Avetisyan et al., 2026; Yang et al., 2026). The vibration behavior of such structures plays a critical role in noise control, vibration mitigation, and structural optimization. Therefore, efficient and accurate calculation of vibration responses in periodic structures during the design stage remains an important and challenging problem (Duhamel and Mencik, 2022).

Conventional deterministic approaches such as Finite Element Analysis (FEA) become computationally prohibitive at mid- and high-frequency. As the frequency increases, the structural wavelength decreases, requiring a substantially increased number of degrees of freedom to maintain spatial resolution and numerical accuracy (Takhchi et al., 2024). This computational burden significantly limits the practical applicability of full deterministic simulations for large-scale structures in the mid-to-high frequency range. To address this limitation, Statistical Energy Analysis (SEA) has been widely adopted as an efficient alternative for calculating energy distribution in complex vibroacoustic systems (Mace, 1995; Lyon and Maidanik, 1962; Lyon, 1974). SEA models a structure as a set of coupled subsystems and characterizes the energy exchange between them through coupling loss factors. Based on the theory of power flow between linearly coupled oscillators (Lyon and Maidanik, 1962), SEA has been successfully applied to many engineering problems, including aircraft fuselage interior noise under turbulent boundary layer excitation, road noise prediction in full-vehicle models, and noise control in large ship structures (Bremner et al., 2002; Lee et al., 2019; Hynnä et al., 1995; Bouhaj et al., 2017). Hybrid FE-SEA approaches have also been developed to extend its applicability toward lower frequencies (Yin and Hopkins, 2013;

Andrade et al., 2022; Fazzolari and Tan, 2020). Despite its efficiency, classical SEA relies heavily on experiment-related parameters, which are often difficult to obtain for complex structural configurations (Fazail et al., 2023).

To overcome this limitation, Virtual Statistical Energy Analysis (VSEA) computes the SEA parameters by using finite element computations instead of performing experiments in a laboratory (Gagliardini et al., 2003; Borello, 2010; Jeong and Park, 2009). This approach not only removes the practical difficulties of setting up physical experiments, but also allows analysts to incorporate energy from all contributing wave types, overcoming the limitations of experimental SEA (Poblet-Puig, 2021). Early theoretical developments established rigorous formulations for estimating coupling loss factors from FEM modal data (Maxit and Guyader, 2001), while the Power Injection Method (PIM) enabled practical identification of internal and coupling loss factors (Bies and Hamid, 1980). VSEA has since been widely used in aerospace, marine, and automotive industries for predicting vibroacoustic responses of complex engineering systems (Borello, 2010). However, when applied to large-scale cylindrical periodic structures, VSEA still faces significant computational challenges. In particular, the determination of valid VSEA frequency bands requires reliable modal density estimation, while the calculation of SEA parameters depends on global modal analysis. Both tasks typically involve extensive eigenvalue extraction and thus lead to substantial computational cost (Zhu et al., 2022; Zhang et al., 2020).

The periodicity of cylindrical structures in engineering practice provides an effective way to improve computational efficiency. In this regard, group theory provides

a powerful means of breaking a large-scale problem into smaller, independent subproblems, thus greatly reducing computational cost. In addition, these subproblems can be solved independently or in parallel, which further enhances computational efficiency (Zingoni, 1997; Peeters and Tromp, 1985; Zingoni, 2015; Kangwai and Guest, 2000). By exploiting the symmetry properties of a structure through group representation theory, the global structural matrices can be transformed into block-diagonal forms. Similarly, Kangwai et al. (1999) showed that group theory enables the stiffness matrix of a symmetric structure to be transformed into a block-diagonal form. Liang et al. presented efficient techniques for studying the dynamic responses of one- and two-dimensional periodic structures (Liang et al., 2018). An algorithm that automatically identifies cyclic symmetries in structures based on nodal connectivity and group-theoretic principles has been presented (Chen et al., 2017). Harth and Michelberger (2016) investigated load determination in quasi-symmetric structures using symmetry components. These studies collectively demonstrate that exploiting structural periodicity can significantly enhance computational efficiency in large-scale structural analyses.

In this paper, an efficient VSEA method is proposed for cylindrical periodic structures based on group theory and the Wittrick-Williams (W-W) algorithm. The global structure is first circumferentially decoupled using group theory, transforming the original coupled eigenvalue problem into independent subproblems. Within this reduced framework, the W-W algorithm (Wittrick and Williams, 1971; Langley and Heron, 1990; Marzani and Viola, 2005; Banerjee and Williams, 1996) is employed to

efficiently compute modal density for frequency-band identification without full modal extraction. Subsequently, a combined W-W and bisection scheme is adopted for efficient modal analysis required for SEA parameter calculation. Finally, the PIM (Mace and Shorter, 2000; Fahy and Ruivo, 1997) is applied to determine internal and coupling loss factors and calculate subsystem energy responses. The proposed framework provides an accurate and computationally efficient solution for modal density calculation, SEA parameter calculation, and vibration response calculation of complex cylindrical periodic structures.

The layout of this paper is as follows. Section 2 reviews the theoretical basis of VSEA and PIM. Section 3 presents the finite element model of the cylindrical periodic structure and the corresponding group-theory-based circumferential decoupling formulation. Section 4 introduces the W-W algorithm for rapid modal counting in frequency-band selection and efficient modal analysis using the bisection method. Section 5 demonstrates the accuracy and computational efficiency of the proposed method through two numerical examples and comparisons with commercial software. Section 6 concludes the paper and discusses future work.

2. Theoretical Formulation of VSEA and PIM

In this paper, we focus on the efficient mid-to-high frequency vibration response analysis of cylindrical periodic structures. The mid-to-high frequency vibration response of engineering structures is commonly analyzed using SEA, in which a

structure is divided into multiple coupled subsystems. For a structure composed of n subsystems, the statistical energy equation can be expressed as (Lyon, 1974)

$$\mathbf{P} = \omega \boldsymbol{\eta} \mathbf{E} \tag{1}$$

where ω is the center frequency of the analysis band, $\mathbf{P}$ is the input power of subsystem matrix, $\mathbf{E}$ is the average energy matrix of subsystem , and $\boldsymbol{\eta}$ is the SEA parameter matrix composed of internal loss factors and coupling loss factors, whose components are given by

$$\boldsymbol{\eta}_{ij} = \begin{cases} \eta_i + \sum_{\substack{j=1 \\ j \neq i}}^{n} \eta_{ij}, & \text{if } i = j \\ -\eta_{ji}, & \text{if } i \neq j \end{cases} \tag{2}$$

The dynamic behavior of the structure is governed by the statistical energy equation Eq (1). The core of SEA is the proper calculation of the SEA parameter matrix. For simple structures, the SEA parameter matrix can usually be obtained from analytical formulas or experimental methods (Mace, 1995). However, such approaches become impractical for complex structures. Consequently, VSEA is employed to identify these SEA parameters using the finite element method (Gagliardini et al., 2003).

A typical VSEA procedure involves subdividing the global structure into subsystems based on the finite element model, selecting a suitable frequency band, and performing modal analysis within this band to obtain natural frequencies and mode shapes. Then, the PIM (Bies and Hamid, 1980) is applied to identify the SEA parameters using the natural frequencies and mode shapes obtained from the modal analysis. In engineering practice including commercial software ACTRAN (Hexagon, 2024), VSEA is typically implemented in the mid-frequency band, where the modal

density (and modal overlap) is sufficient to satisfy the statistical assumptions of SEA. The SEA parameters identified in this range are interpolated or extrapolated to calculate vibration energy responses at higher frequencies. Therefore, it is very important to select an appropriate mid-frequency band and extracting the corresponding modal information which is essential for SEA parameter calculation. The formulation of the PIM used to calculate these SEA parameters is summarized below(Bies and Hamid, 1980; Mace and Shorter, 2000).

The undamped free vibration equation of the global structure is written as

$$\mathbf{M}\ddot{\mathbf{u}}(t)+\mathbf{K}\mathbf{u}(t)=0 \tag{3}$$

where $\mathbf{M}$ and $\mathbf{K}$ denote the global mass and stiffness matrices, respectively, and $\mathbf{u}(t)$ is the generalized displacement vector. Assuming harmonic motion yields the generalized eigenvalue problem

$$(\mathbf{K}-\omega_m{}^2\mathbf{M})\boldsymbol{\phi}_m=\mathbf{0} \tag{4}$$

where ω_m is the m-th natural frequency and $\boldsymbol{\phi}_m$ is the associated mode shape. To project the global modal energy to each subsystem, the subsystem stiffness distribution matrix and mass distribution matrix are introduced. For subsystem r, with stiffness matrix $\mathbf{K}_r$, mass matrix $\mathbf{M}_r$, and transformation matrix $\mathbf{Z}_r$, the corresponding distribution matrices are given by (Mace and Shorter, 2000)

$$\begin{aligned}\bar{\mathbf{K}}_r&=\boldsymbol{\phi}^{\mathrm{T}}\mathbf{Z}_r\mathbf{K}_r\mathbf{Z}_r{}^{\mathrm{T}}\boldsymbol{\phi}\\ \bar{\mathbf{M}}_r&=\boldsymbol{\phi}^{\mathrm{T}}\mathbf{Z}_r\mathbf{M}_r\mathbf{Z}_r{}^{\mathrm{T}}\boldsymbol{\phi}\end{aligned} \tag{5}$$

Within the VSEA framework, the global structural response under virtual excitation is described using modal admittance. For the m-th mode, the modal admittance is expressed as

$$\alpha_m = \frac{1}{\omega_m^2(1+\mathrm{i}\xi)-\omega^2} \tag{6}$$

where α_m denotes the admittance corresponding to the *m*-th mode, ω_m is the *m*-th natural frequency, ξ is the structural damping ratio, i is the imaginary unit, and ω is the center frequency of the analysis frequency band. A rain-on-the-roof type excitation (Mace and Shorter, 2000) is adopted as the virtual excitation, which represents a spatially delta-correlated and frequency-independent random load applied over the subsystem region. In modal coordinates, the projected virtual excitation is written as

$$\mathbf{Q}_f = \boldsymbol{\phi}^{\mathrm{T}}\mathbf{Z}_r\mathbf{M}_r\mathbf{Z}_r{}^{\mathrm{T}}\boldsymbol{\phi} \tag{7}$$

The input power of subsystem *r* is given by

$$P_{in} = \frac{1}{2}\mathrm{Re}\left\{i\omega\sum_m \mathbf{Q}_{f,mm}\alpha_m\right\} \tag{8}$$

where m denotes the number of selected modes, and $\mathbf{Q}_{f,mm}$ is the element in the *m*-th row and *m*-th column of the load matrix. For subsystem *r*, the kinetic and potential energies are calculated as

$$\begin{aligned} V_r &= \sum_m \mathbf{Q}_{f,mp}\mathbf{k}_{r,mp}\Gamma_{mp} \\ T_r &= \omega^2\sum_m \mathbf{Q}_{f,mp}\mathbf{m}_{r,mp}\Gamma_{mp} \\ \Gamma_{mp} &= \frac{1}{4}\alpha_m^*\alpha_p \end{aligned} \tag{9}$$

The total energy of each subsystem is the sum of its kinetic and potential energies which can be expressed as

$$E_r = V_r + T_r = \frac{1}{4}\sum_{m,p}\mathbf{Q}_{f,mp}\mathbf{k}_{r,mp}\alpha_m^*\alpha_p + \frac{1}{4}\omega^2\sum_{m,p}\mathbf{Q}_{f,mp}\mathbf{m}_{r,mp}\alpha_m^*\alpha_p \tag{10}$$

where V_r and T_r denote the kinetic and potential energies, $\mathbf{k}_r = \boldsymbol{\phi}^{\mathrm{T}}\mathbf{Z}_r\mathbf{K}_r\mathbf{Z}_r^T\boldsymbol{\phi}$, $\mathbf{m}_r = \boldsymbol{\phi}^{\mathrm{T}}\mathbf{Z}_r\mathbf{M}_r\mathbf{Z}_r^T\boldsymbol{\phi}$, and $\mathbf{k}_{r,mp}$ represents the (m, p)-th element of matrix $\mathbf{k}_r$, $\mathbf{m}_{r,mp}$ represents the (m, p)-th element of matrix $\mathbf{m}_r$. α_m^* is the adjugate of the admittance α_m corresponding to the m-th order mode. To ensure statistical stability, the power P_{in} and these energies are integrated and averaged over the analysis frequency band, which yields (Mace and Shorter, 2000)

$$\begin{aligned} \overline{V} &= \left(\frac{1}{4B}\right)\sum_m \omega_m^2 Q'_{f,mm} J_{1,m}, J_{1,m} = \int_\Omega |\alpha_m|^2 \mathrm{d}\omega \\ \overline{T} &= \left(\frac{1}{4B}\right)\sum_m Q'_{f,mm} J_{2,m}, J_{2,m} = \int_\Omega \omega^2 |\alpha_m|^2 \mathrm{d}\omega \end{aligned} \tag{11}$$

$$\begin{aligned} \overline{V}_r &= \left(\frac{1}{4B}\right)\sum_{m,p} Q'_{f,mp} \boldsymbol{\kappa}_{r,mp} J_{4,mp}, J_{4,mp} = \int_\Omega \alpha_m^* \alpha_p \mathrm{d}\omega \\ \overline{T}_r &= \left(\frac{1}{4B}\right)\sum_{m,p} Q'_{f,mp} \boldsymbol{\mu}_{r,mp} J_{5,mp}, J_{5,mp} = \int_\Omega \omega^2 \alpha_m^* \alpha_p \mathrm{d}\omega \\ \overline{P}_{in} &= \left(\frac{1}{2B}\right)\sum_m Q'_{f,mm} J_{3,m}, J_{3,m} = \int_\Omega \mathrm{Re}\{i\omega\alpha_m\} \mathrm{d}\omega \end{aligned} \tag{12}$$

To illustrate the parameter calculation procedure of the PIM, consider a system consisting of two subsystems. A frequency band $\Delta\omega$ is selected, and virtual power is injected separately into subsystems 1 and 2. The subsystem energies are calculated using $E_r = \overline{V}_r + \overline{T}_r$, and $\overline{P}_{in}$ is used to calculate P_r. Injecting power into subsystem 1 yields

$$\begin{bmatrix} P_1 \\ 0 \end{bmatrix} = \omega \cdot \boldsymbol{\eta} \begin{bmatrix} E_{11} \\ E_{21} \end{bmatrix} \tag{13}$$

Injecting power into subsystem 2 yields

$$\begin{bmatrix} 0 \\ P_2 \end{bmatrix} = \omega \cdot \boldsymbol{\eta} \begin{bmatrix} E_{12} \\ E_{22} \end{bmatrix} \tag{14}$$

By combining Eq. (13) and Eq. (14), the power-energy relationship can be written in matrix form as

$$\mathbf{P}=\begin{bmatrix} P_1 & 0 \\ 0 & P_2 \end{bmatrix}=\omega\cdot\boldsymbol{\eta}\begin{bmatrix} E_{11} & E_{12} \\ E_{21} & E_{22} \end{bmatrix} \tag{15}$$

from which the SEA parameter matrix is directly obtained as

$$\boldsymbol{\eta}=\frac{1}{\omega}\mathbf{P}\begin{bmatrix} E_{11} & E_{12} \\ E_{21} & E_{22} \end{bmatrix}^{-1} \tag{16}$$

The above analysis establishes the procedure for calculating the SEA parameter matrix through the PIM. In practical implementation of VSEA, two key steps are required. The first is the identification of a proper mid-frequency band, which requires the evaluation of modal density to verify the statistical validity of SEA. The second is the calculation of the SEA parameter matrix, which depends on modal analysis for extracting the natural frequencies and mode shapes within the selected frequency band. For large-scale cylindrical periodic structures, both tasks involve large finite element models and become computationally demanding. To improve the efficiency of both modal density evaluation and modal analysis, a circumferential decoupling approach based on group theory and modal density calculation and modal analysis based on the W-W algorithm are introduced in the following section.

3. Circumferential Decoupling of Cylindrical Periodic Structures Based on Group Theory

Large-scale cylindrical periodic structures exhibit cyclic symmetry in the circumferential direction. By exploiting this property, group theory is employed to

decouple the system dynamic equations in the circumferential direction, whereby the original large-scale eigenvalue problem is transformed into a set of independent smaller subproblems. This treatment significantly reduces computational cost while preserving modal accuracy. The detailed formulation of the circumferential decoupling procedure is presented below.

As shown in Fig. 1, the unit cell is translated N times to form a one-dimensional strip periodic structure consisting of N identical cells, and the strip structure is rotated and replicated M times about the central axis in the circumferential direction, resulting in the complete cylindrical periodic structure. As all unit cells have identical geometric and material properties, the global cylindrical periodic structure can be obtained by first assembling the strip structure in the axial direction and then assembling the structure in the circumferential direction.

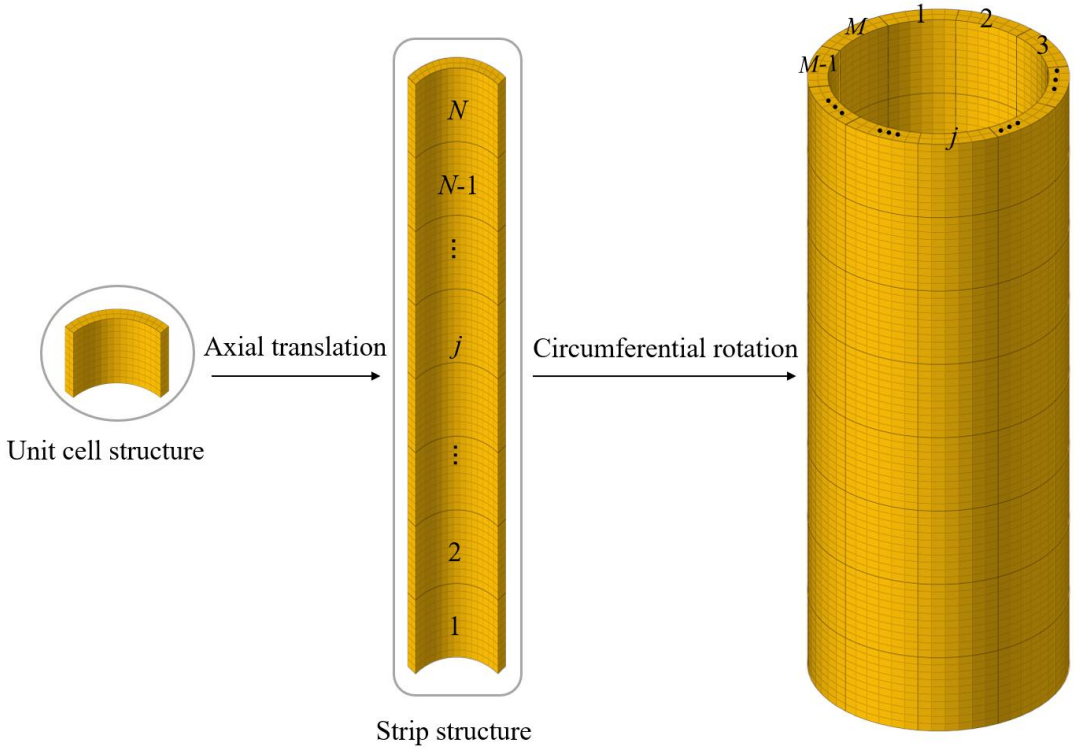


Fig. 1 Schematic diagram of cylindrical periodic structure.

To fully exploit the repetitive symmetry of cylindrical periodic structures in both the axial and circumferential directions, it is necessary to systematically classify the nodal degrees of freedom within each unit cell. The nodal grouping scheme for the unit cells forming the structure is described below. For the *n*-th unit cell in the *m*-th strip structure, denoted as unit cell $\{m, n\}$, the nodes are partitioned into nine mutually exclusive sets according to their geometric locations, as illustrated in Fig. 2. Let the numbers of nodes in groups *a*, *b*, *c*, and *i* be denoted by d_a、d_b、d_c and d_i, respectively, with $d_1 = d_a + d_b + d_c + d_i$、$d_2 = Nd_1 + d_a + d_b$、$d_3 = d_a + d_b$.

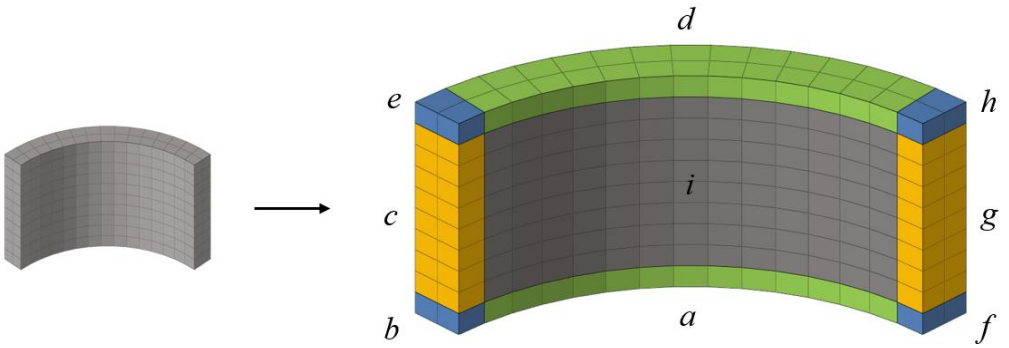


Fig. 2 Schematic diagram of unit cell node grouping.

Based on the above nodal grouping scheme, the unit-cell stiffness matrix $\mathbf{K}_{cell}$ and mass matrix $\mathbf{M}_{cell}$ can be naturally expressed in block-matrix form composed of multiple submatrices. Taking the stiffness matrix $\mathbf{K}_{cell}$ as an example, it can be written as

$$\mathbf{K}_{cell} = \left[\mathbf{K}_{pq}\right] = \begin{bmatrix} \mathbf{K}_{aa} & \cdots & \mathbf{K}_{ai} \\ \vdots & & \vdots \\ \mathbf{K}_{ia} & \cdots & \mathbf{K}_{ii} \end{bmatrix} \quad p,q \in \{a,b,c,d,e,f,g,h,i\} \tag{17}$$

where $\mathbf{K}_{pq}$ denotes the submatrix between the *p*-th and *q*-th nodal groups.

For the global structure, the degrees of freedom are organized according to the M circumferential strips. Consequently, the stiffness matrix $\mathbf{K}$ and mass matrix $\mathbf{M}$ can both be represented as block matrices composed of $M \times M$ subblocks. Due to the cyclic symmetry in the circumferential direction, each row or column of the blocks can be obtained by a shift of the preceding ones, exhibiting a cyclic manner globally. Consequently, matrices with such structure are called block-circulant matrices. The global stiffness matrix $\mathbf{K}$ can be written in the following equivalent form

$$\mathbf{K}=\begin{bmatrix} \mathbf{K}_I^0+\mathbf{K}_{II}^0 & \mathbf{K}_{III}^0 & \mathbf{0} & \cdots & \mathbf{0} & \left(\mathbf{K}_{III}^0\right)^{\mathrm{T}} \\ \left(\mathbf{K}_{III}^0\right)^{\mathrm{T}} & \mathbf{K}_I^0+\mathbf{K}_{II}^0 & \mathbf{K}_{III}^0 & \mathbf{0} & \cdots & \mathbf{0} \\ \mathbf{0} & \left(\mathbf{K}_{III}^0\right)^{\mathrm{T}} & \mathbf{K}_I^0+\mathbf{K}_{II}^0 & \ddots & \ddots & \vdots \\ \vdots & \mathbf{0} & \ddots & \ddots & \ddots & \mathbf{0} \\ \mathbf{0} & \vdots & \ddots & \ddots & \mathbf{K}_I^0+\mathbf{K}_{II}^0 & \mathbf{K}_{III}^0 \\ \mathbf{K}_{III}^0 & \mathbf{0} & \cdots & \mathbf{0} & \left(\mathbf{K}_{III}^0\right)^{\mathrm{T}} & \mathbf{K}_I^0+\mathbf{K}_{II}^0 \end{bmatrix} \tag{18}$$

where $\mathbf{K}_i^0\left(i=I,II,III\right)$ is a matrix of $d_2 \times d_2$ dimension and has the following block structure

$$\mathbf{K}_i^0=\begin{bmatrix} \mathbf{K}_i^1 & \mathbf{K}_i^3 & \mathbf{0} & \cdots & \mathbf{0} & \mathbf{0} \\ \mathbf{K}_i^4 & \mathbf{K}_i^1+\mathbf{K}_i^2 & \mathbf{K}_i^3 & \mathbf{0} & \cdots & \mathbf{0} \\ \mathbf{0} & \mathbf{K}_i^4 & \mathbf{K}_i^1+\mathbf{K}_i^2 & \ddots & \ddots & \vdots \\ \vdots & \mathbf{0} & \ddots & \ddots & \mathbf{K}_i^3 & \mathbf{0} \\ \mathbf{0} & \vdots & \ddots & \mathbf{K}_i^4 & \mathbf{K}_i^1+\mathbf{K}_i^2 & \mathbf{K}_i^6 \\ \mathbf{0} & \mathbf{0} & \cdots & \mathbf{0} & \mathbf{K}_i^7 & \mathbf{K}_i^5 \end{bmatrix} \tag{19}$$

where the submatrices $\mathbf{K}_i^m\left(i=I,II,III;\ m=1,\ 2,\ 3,\ \cdots,\ 7\right)$ represent the stiffness coupling between unit cells as detailed in the Appendix A. The mass matrix $\mathbf{M}$ also has the same block matrix form as the stiffness matrix $\mathbf{K}$. The dynamic stiffness matrix of the cylindrical periodic structure is defined as $\mathbf{R}=(\mathbf{K}-\omega^2\mathbf{M})$ which also has the same block matrix form.

According to group theory, there exists an orthogonal transformation matrix by which $\mathbf{R}$ can be block-diagonalized. The corresponding orthogonal transformation matrix $\mathbf{T}_M$ is expressed as

$$\mathbf{T}_M = \frac{1}{\sqrt{M}} \begin{bmatrix} 1 & 1 & 1 & \cdots & 1 \\ 1 & \varepsilon & \varepsilon^2 & \cdots & \varepsilon^{M-1} \\ 1 & \varepsilon^2 & \varepsilon^4 & \cdots & \varepsilon^{2(M-1)} \\ \vdots & \vdots & \vdots & \ddots & \vdots \\ 1 & \varepsilon^{M-1} & \varepsilon^{2(M-1)} & \cdots & \varepsilon^{(M-1)^2} \end{bmatrix} \tag{20}$$

where $\varepsilon = \exp\left(-\mathrm{i}2\pi/M\right)$. After applying this orthogonal transformation, the matrix $\mathbf{R}$ can be altered as

$$\bar{\mathbf{R}} = \left(\mathbf{T}_M^{\mathrm{H}} \otimes \mathbf{I}_{d_2}\right) \mathbf{R} \left(\mathbf{T}_M \otimes \mathbf{I}_{d_2}\right) \tag{21}$$

In Eq. (21), $\mathbf{I}_{d_2}$ is the identity matrix with an order of $d_2 \times d_2$. According to group theory, the matrix $\bar{\mathbf{R}}$ becomes block-diagonal and can be written as follows:

$$\bar{\mathbf{R}} = \mathrm{diag}\left(\bar{\mathbf{R}}_m\right) \ \left(m = 1, 2, \cdots, M\right) \tag{22}$$

In which, the *m*-th sub-block $\bar{\mathbf{R}}_m$ can be given that

$$\bar{\mathbf{R}}_m = \mathbf{R}_I^0 + \varepsilon^{m-1} \mathbf{R}_{II}^0 + \varepsilon^{1-m} \left(\mathbf{R}_{II}^0\right)^{\mathrm{T}} \tag{23}$$

Here, the expression of the matrix $\mathbf{R}_i^0 \ \left(i = I, II\right)$ is similar to $\mathbf{K}_i^0$ given in Eq. (19).

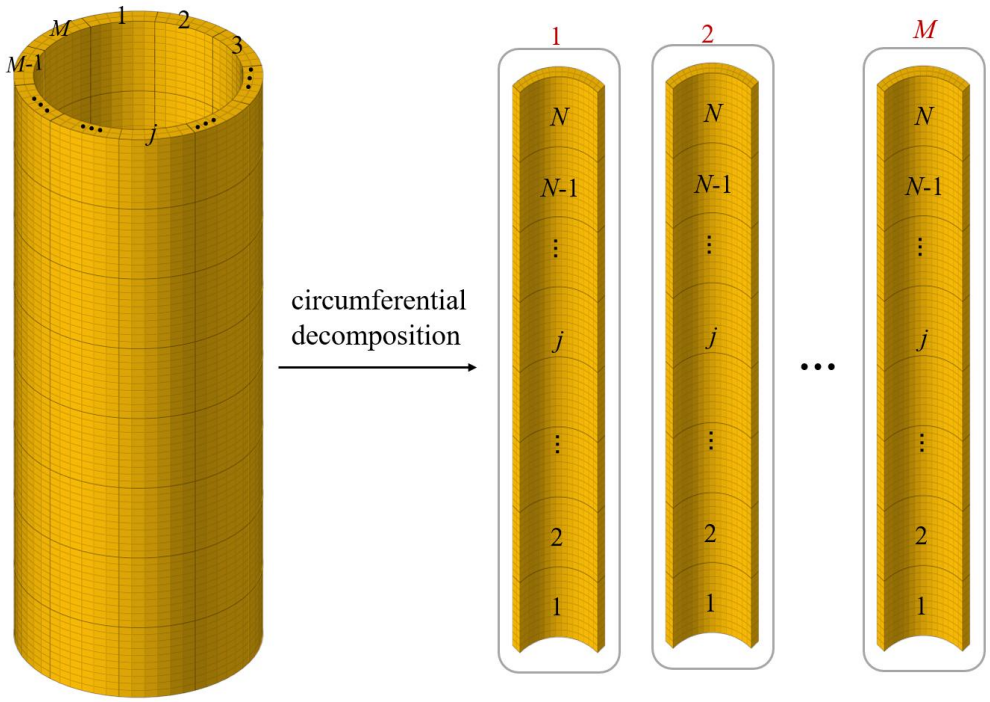


Fig. 3 Circumferential decoupling of a cylindrical periodic structure.

Through the above transformation, the large-scale eigenvalue problem of the cylindrical periodic structure is converted into a series of independent subproblems, as illustrated in Fig. 3. This decoupled formulation provides the basis for efficient modal density evaluation and modal analysis, which are required for valid frequency-band identification and SEA parameter calculation. The corresponding solution procedure based on the W-W algorithm is presented in the following section.

4. Modal Density Calculation and Modal Analysis Based on the W-W Algorithm

In Section 3, the cylindrical periodic structure was circumferentially decoupled using group theory, reducing the original eigenvalue problem to a set of independent one-dimensional periodic subproblems. However, each reduced subproblem remains

periodic in the axial direction. To efficiently determine the modal information required for VSEA, the W-W algorithm is employed to evaluate eigenvalue counts and locate natural frequencies directly from the dynamic stiffness matrices without explicit eigenvalue decomposition. On this basis, modal density is first calculated for frequency-band selection, and then natural frequencies and mode shapes are extracted for subsequent SEA parameter calculation.

4.1 Modal Density Calculation

Modal density serves as a fundamental criterion for assessing the applicability of SEA. Conventional approaches determine modal density through explicit eigenvalue extraction followed by modal counting, which becomes prohibitively expensive for large-scale periodic systems. The W-W algorithm circumvents this limitation by directly evaluating the number of eigenvalues below a prescribed frequency without solving the eigenvalue problem explicitly. The total modal count is expressed as (Wittrick and Williams, 1971)

$$J(\omega_{\#}) = \sum_{i=1}^{m} J_i(\omega_{\#}) + \operatorname{sign}\left\{\mathbf{R}(\omega_{\#})\right\} \tag{24}$$

where $J(\omega_{\#})$ denotes the number of eigenvalues below frequency $\omega_{\#}$, m is the number of substructures, $J_i(\omega_{\#})$ represents the eigenvalue count of the i-th substructure, $\mathbf{R}(\omega_{\#})$ is the assembled boundary dynamic stiffness matrix of all substructures, and $\operatorname{sign}\{\#\}$ denotes the number of negative eigenvalues of a matrix.

For the cylindrical periodic structure considered in this paper, after circumferential decoupling, each independent subproblem corresponds to a one-dimensional periodic

structure whose dynamic behavior can be represented by an equivalent system matrix assembled from unit-cell matrices. For any one of these one-dimensional periodic structures, the global matrix is constructed by assembling the condensed unit-cell matrix $\bar{\mathbf{K}}_{cell}$ according to Eq. (23), which takes the form

$$\bar{\mathbf{K}}_{cell} = \begin{bmatrix} \bar{\mathbf{K}}^{1} & \bar{\mathbf{K}}^{2} \\ \bar{\mathbf{K}}^{3} & \bar{\mathbf{K}}^{4} \end{bmatrix} \tag{25}$$

where the matrix $\bar{\mathbf{K}}^{i}\ \left(i=1,2,3,4\right)$ can be written as

$$\begin{aligned} \bar{\mathbf{K}}^{1} &= \mathbf{K}_{I}^{1} + \varepsilon^{m-1}\mathbf{K}_{II}^{1} + \varepsilon^{1-m}\left(\mathbf{K}_{II}^{1}\right)^{\mathrm{T}} \\ \bar{\mathbf{K}}^{2} &= \mathbf{K}_{I}^{6} + \varepsilon^{m-1}\mathbf{K}_{II}^{6} + \varepsilon^{1-m}\left(\mathbf{K}_{II}^{7}\right)^{\mathrm{T}} \\ \bar{\mathbf{K}}^{3} &= \mathbf{K}_{I}^{7} + \varepsilon^{m-1}\mathbf{K}_{II}^{7} + \varepsilon^{1-m}\left(\mathbf{K}_{II}^{6}\right)^{\mathrm{T}} \\ \bar{\mathbf{K}}^{4} &= \mathbf{K}_{I}^{5} + \varepsilon^{m-1}\mathbf{K}_{II}^{5} + \varepsilon^{1-m}\left(\mathbf{K}_{II}^{5}\right)^{\mathrm{T}} \end{aligned} \tag{26}$$

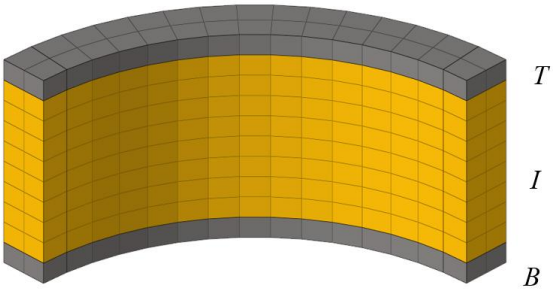


Fig. 4 Schematic of node reorganization for condensation.

For convenience in the subsequent derivation, node groups *a* and *b* in Fig. 2 are combined to form a new group *B*; similarly, node groups *c* and *i* are merged into *I*, and node groups *d* and *e* are merged into *T*, as illustrated in Fig. 4. Under this revised node grouping scheme, the stiffness matrix $\bar{\mathbf{K}}_{cell}$ in Eq. (25), mass matrix of the unit cell can be rewritten in block form, then the dynamic stiffness matrix of the unit cell $\mathbf{R}_{cell} = \bar{\mathbf{K}}_{cell} - \omega^{2}\bar{\mathbf{M}}_{cell}$ is given as

$$\mathbf{R}_{cell}=\begin{bmatrix}\mathbf{R}_{BB} & \mathbf{R}_{BI} & \mathbf{R}_{BT}\\ \mathbf{R}_{IB} & \mathbf{R}_{II} & \mathbf{R}_{IT}\\ \mathbf{R}_{TB} & \mathbf{R}_{TI} & \mathbf{R}_{TT}\end{bmatrix} \tag{27}$$

After completing the condensation of degrees of freedom, the corresponding relationship between the displacement vector and the force vector is

$$\begin{bmatrix}\mathbf{p}_B\\ \mathbf{p}_T\end{bmatrix}=\mathbf{R}_{cell}\begin{bmatrix}\mathbf{q}_B\\ \mathbf{q}_T\end{bmatrix}=\begin{bmatrix}\mathbf{R}_{cell}^{11} & \mathbf{R}_{cell}^{12}\\ \mathbf{R}_{cell}^{21} & \mathbf{R}_{cell}^{22}\end{bmatrix}\begin{bmatrix}\mathbf{q}_B\\ \mathbf{q}_T\end{bmatrix} \tag{28}$$

where

$$\begin{bmatrix}\mathbf{R}_{cell}^{11} & \mathbf{R}_{cell}^{12}\\ \mathbf{R}_{cell}^{21} & \mathbf{R}_{cell}^{22}\end{bmatrix}=\begin{bmatrix}\mathbf{R}_{BB}-\mathbf{R}_{BI}\left(\mathbf{R}_{II}\right)^{-1}\mathbf{R}_{IB} & \mathbf{R}_{BT}-\mathbf{R}_{TI}\left(\mathbf{R}_{II}\right)^{-1}\mathbf{R}_{IT}\\ \mathbf{R}_{TL}-\mathbf{R}_{TI}\left(\mathbf{R}_{II}\right)^{-1}\mathbf{R}_{IB} & \mathbf{R}_{TT}-\mathbf{R}_{TI}\left(\mathbf{R}_{II}\right)^{-1}\mathbf{R}_{IT}\end{bmatrix} \tag{29}$$

$$\mathbf{R}_{cell}^{11}=\left(\mathbf{R}_{cell}^{11}\right)^{\mathrm{T}},\quad \mathbf{R}_{cell}^{22}=\left(\mathbf{R}_{cell}^{22}\right)^{\mathrm{T}},\quad \mathbf{R}_{cell}^{12}=\left(\mathbf{R}_{cell}^{21}\right)^{\mathrm{T}} \tag{30}$$

The governing equation of cell k and $k+1$ can be expressed as

$$\begin{bmatrix}-\mathbf{p}_{k-1}\\ \mathbf{p}_k\end{bmatrix}=\begin{bmatrix}\mathbf{R}_{k-1,k}^{11} & \mathbf{R}_{k-1,k}^{12}\\ \mathbf{R}_{k-1,k}^{21} & \mathbf{R}_{k-1,k}^{22}\end{bmatrix}\begin{bmatrix}\mathbf{q}_{k-1}\\ \mathbf{q}_k\end{bmatrix} \tag{31}$$

$$\begin{bmatrix}-\mathbf{p}_{k}\\ \mathbf{p}_{k+1}\end{bmatrix}=\begin{bmatrix}\mathbf{R}_{k-1,k+1}^{11} & \mathbf{R}_{k-1,k+1}^{12}\\ \mathbf{R}_{k-1,k+1}^{21} & \mathbf{R}_{k-1,k+1}^{22}\end{bmatrix}\begin{bmatrix}\mathbf{q}_{k}\\ \mathbf{q}_{k+1}\end{bmatrix} \tag{32}$$

From Eq. (31) and Eq. (32), eliminating $\mathbf{q}_k$ and $\mathbf{p}_k$ gives

$$\begin{bmatrix}-\mathbf{p}_{k-1}\\ \mathbf{p}_{k+1}\end{bmatrix}=\begin{bmatrix}\mathbf{R}_{k-1,k+1}^{11} & \mathbf{R}_{k-1,k+1}^{12}\\ \mathbf{R}_{k-1,k+1}^{21} & \mathbf{R}_{k-1,k+1}^{22}\end{bmatrix}\begin{bmatrix}\mathbf{q}_{k-1}\\ \mathbf{q}_{k+1}\end{bmatrix} \tag{33}$$

where

$$\begin{aligned}
\mathbf{R}_{k-1,k+1}^{11}&=\mathbf{R}_{k-1,k}^{11}-\mathbf{R}_{k-1,k}^{12}\left(\mathbf{R}_{k-1,k}^{22}+\mathbf{R}_{k,k+1}^{11}\right)^{-1}\mathbf{R}_{k-1,k}^{21}\\
\mathbf{R}_{k-1,k+1}^{12}&=\left(\mathbf{R}_{k-1,k+1}^{21}\right)^{\mathrm{T}}=-\mathbf{R}_{k-1,k}^{12}\left(\mathbf{R}_{k-1,k}^{22}+\mathbf{R}_{k,k+1}^{11}\right)^{-1}\mathbf{R}_{k,k+1}^{12}\\
\mathbf{R}_{k-1,k+1}^{22}&=\mathbf{R}_{k,k+1}^{22}-\mathbf{R}_{k,k+1}^{21}\left(\mathbf{R}_{k-1,k}^{22}+\mathbf{R}_{k,k+1}^{11}\right)^{-1}\mathbf{R}_{k,k+1}^{12}
\end{aligned} \tag{34}$$

As shown in Fig. 5, the dynamic stiffness matrices of the two unit cells arranged in the axial direction are denoted by $\mathbf{R}_{1,2}$ and $\mathbf{R}_{2,3}$, and $\mathbf{R}_{1,2}=\mathbf{R}_{2,3}=\mathbf{R}_{cell}$. For the substructure formed by two adjacent unit cells with both ends fixed, its eigenvalue

count is

$$J_{1,3}^{\text{C-C}} = 2J_{\text{sub}}^{\text{C-C}} + \text{sign}\left\{\mathbf{R}_{1,2}^{22} + \mathbf{R}_{2,3}^{11}\right\} \tag{35}$$

where $J_{\text{sub}}^{\text{C-C}} = \text{sign}\left\{\mathbf{R}_{II}\right\}$ denotes the eigenvalue count of a single unit cell with both ends fixed. The outlet dynamic stiffness matrix $\mathbf{R}_{1,3}$ of the substructure composed of two unit cells can be obtained from Eq. (32). Next, let $J_{\text{sub}}^{\text{C-C}} = J_{1,3}^{\text{C-C}}$, $\mathbf{R}_{1,2} = \mathbf{R}_{1,3}$, and $\mathbf{R}_{2,3} = \mathbf{R}_{1,3}$, and then the eigenvalue count and dynamic stiffness matrix of the substructure formed by four unit cells can be obtained using Eq. (34) and Eq. (35). Following this procedure, the eigenvalue count of the overall structure composed of 2^N unit cells can be obtained. It is worth noting that the 2^N doubling scheme is introduced for computational efficiency and the W-W algorithm itself is applicable to structures with an arbitrary number of unit cells, and the eigenvalue count can be calculated without requiring the system size to follow the 2^N form.

Based on the eigenvalue counting method described above, the modal density $n(\omega)$ at the center frequency ω can be further solved by calculating the ratio of the number of modes within a given frequency band $[\omega_1, \omega_2]$ to the bandwidth, as follows (Lyon, 1974)

$$n(\omega) \approx \frac{J(\omega_2) - J(\omega_1)}{\omega_2 - \omega_1} \tag{36}$$

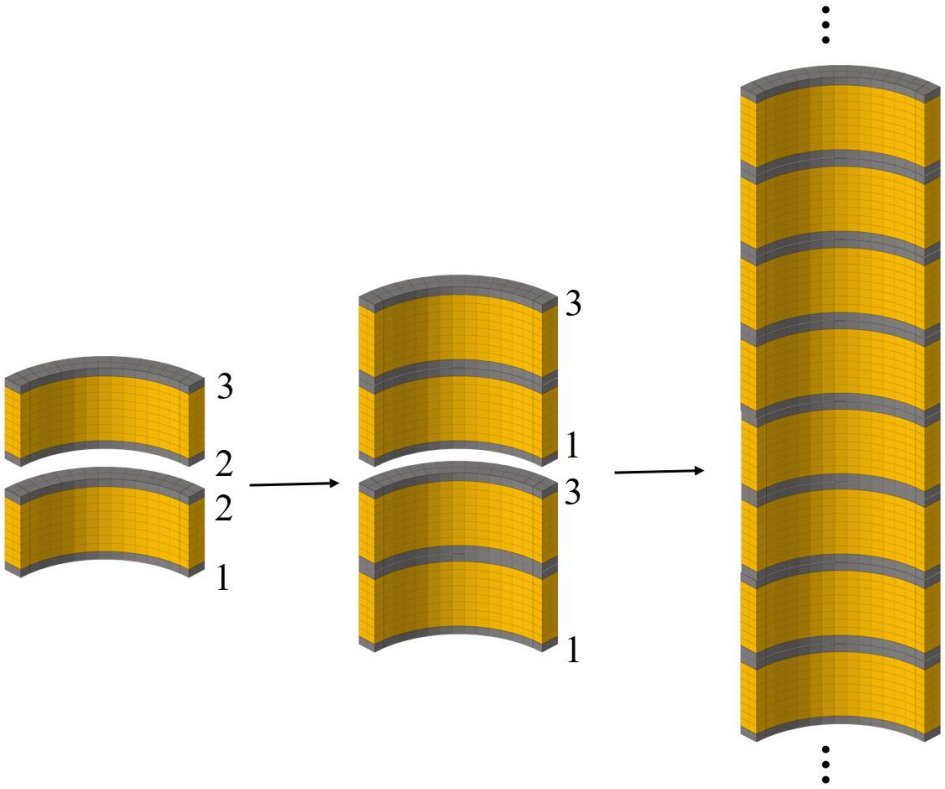


Fig. 5 Assembly and doubling process of unit-cell dynamic stiffness matrices.

4.2 Modal Analysis Procedure

Following the circumferential decoupling described in the previous section, the original eigenvalue problem of the cylindrical periodic structure is transformed into a set of independent sub-eigenvalue problems. In order to calculate the modal characteristics required for subsequent VSEA parameter calculation, an efficient modal analysis procedure is employed based on the W-W algorithm. The natural frequencies and corresponding mode shapes of each circumferential one-dimensional periodic substructure are first computed and then assembled to reconstruct the physical modal solutions of the entire cylindrical periodic structure.

For the *m*-th circumferential one-dimensional periodic substructure, within the W-W framework, by calculating the eigenvalue count $J(\omega)$ at a given frequency ω, the number of eigenvalues below that frequency can be determined. For a prescribed frequency band (ω_a, ω_b), the total number of eigenfrequencies within the band is given by $N = J(\omega_b) - J(\omega_a)$. If $N > 1$, the frequency band is recursively subdivided into smaller bands until each sub-band contains only a single natural frequency. For $N = 1$, exactly one natural frequency exists within this frequency band. Based on this criterion, a bisection search strategy is employed to locate the natural frequency. The midpoint frequency $\omega_c = (\omega_a + \omega_b)/2$ of the current frequency band is selected, and the corresponding eigenvalue count $J(\omega_c)$ is computed. If $J(\omega_c) - J(\omega_a) = 1$, the natural frequency lies in $[\omega_a, \omega_c]$; otherwise, it lies in $[\omega_c, \omega_b]$.This process is repeated until the bandwidth satisfies a prescribed tolerance, yielding the natural frequency. This procedure involves only algebraic operations on the dynamic stiffness matrix and sign counting, without computing eigenvectors. This leads to high numerical efficiency, particularly for high-order modes or densely spaced eigenfrequencies.

Once the natural frequency $\omega_{\#}$ are obtained, the corresponding eigenvalue equation can be written as

$$\mathbf{R}_m(\omega_{\#})\boldsymbol{\phi}_m = \mathbf{0} \tag{37}$$

For this frequency, the system matrix becomes singular and admits a nontrivial null-space solution $\boldsymbol{\phi}_m$. In numerical implementation, the modal shape of the one-dimensional periodic substructure can be obtained by solving the underdetermined linear system with an appropriate normalization constraint. After determining the mode

shapes of all circumferential subsystems, the physical mode shapes of the entire cylindrical periodic structure can be reconstructed through the inverse group-theory transformation.

In summary, the W-W algorithm provides an efficient framework for determining the modal characteristics of the decoupled one-dimensional periodic substructures. The resulting modal density is used to identify valid analysis frequency bands, while the extracted natural frequencies and reconstructed mode shapes provide the modal information required for subsequent SEA parameter calculation.

5. Numerical Example

In this section, two cylindrical periodic structures are selected as numerical case studies to validate the accuracy and efficiency of the proposed method. These examples are designed to demonstrate its applicability to both multi-material cylindrical shells and more complex periodic sandwich structures. The method is systematically evaluated from three perspectives: efficient modal density calculation, the accuracy and efficiency of modal analysis, and energy response calculation. All numerical simulations were performed on a desktop workstation equipped with a single Intel® Xeon® CPU Silver 4116 processor (2.10 GHz) and 64 GB of RAM. Finite element models for all numerical cases were constructed using commercial finite element software, and results were compared against those obtained from NASTRAN and ACTRAN under identical material properties and boundary conditions. To assess the accuracy of the proposed method, the relative error e of the natural frequencies is

defined as

$$e = \frac{\left| f_{\mathrm{P}} - f_{\mathrm{N}} \right|}{f_{\mathrm{N}}} \times 100\% \tag{38}$$

where f_{P} and f_{N} denote the natural frequencies obtained by the proposed method and NASTRAN, respectively. Additionally, the Modal Assurance Criterion (MAC) is employed to evaluate the consistency of the mode shapes. The MAC for two mode shapes is defined as

$$\mathrm{MAC} = \frac{\left| \boldsymbol{\phi}_{\mathrm{P}}^{\mathrm{T}} \boldsymbol{\phi}_{\mathrm{N}} \right|^2}{\left(\boldsymbol{\phi}_{\mathrm{P}}^{\mathrm{T}} \boldsymbol{\phi}_{\mathrm{P}} \right) \left(\boldsymbol{\phi}_{\mathrm{N}}^{\mathrm{T}} \boldsymbol{\phi}_{\mathrm{N}} \right)} \tag{39}$$

where $\boldsymbol{\phi}_{\mathrm{P}}$ and $\boldsymbol{\phi}_{\mathrm{N}}$ denote the mode shapes obtained by the proposed method and NASTRAN, respectively.

5.1 Example 1: Composite Cylindrical Shell

As shown in Fig. 6 (a), a cylindrical shell with a height of 2.56 m, radius of 0.5 m, and thickness of 0.05 m is considered. The cylindrical shell is longitudinally partitioned into four distinct material regions: aluminum, magnesium, titanium, and steel. The material properties of the cylindrical shell are listed in Table 1. The cylindrical shell is discretized into approximately 1.66 million degrees of freedom, with about 460000 elements and 550000 nodes, and a minimum solid element size of 0.01 m. As shown in Fig. 6 (b), the cylindrical structure is subdivided into four subsystems according to the axial distribution of material.

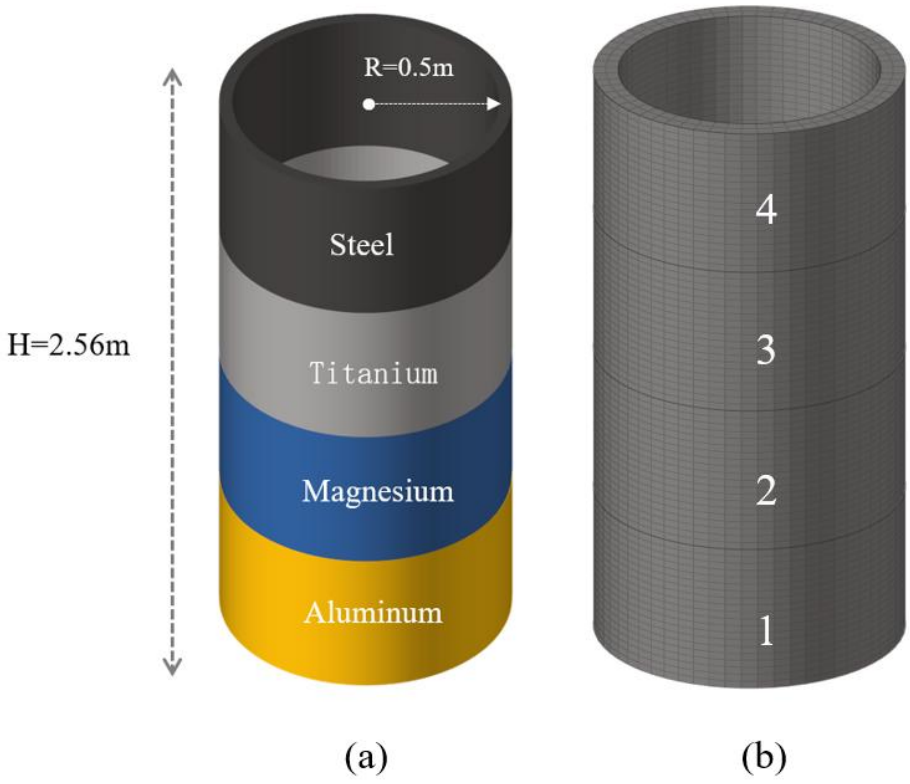


Fig. 6 Composite cylindrical shell model and subsystem partitioning.

Table 1 Materials of the cylindrical shell.

Material	Young's modulus (Pa)	Density (kg/m^3)	Poisson's ratio
Aluminum	7.2E10	2700	0.33
Magnesium	4.5E10	1740	0.35
Titanium	1.1E11	4500	0.34
Steel	2.1E11	7850	0.30

The modal density of the structure is first evaluated within standard one-third-octave bands up to 8 kHz to identify the frequency range where SEA assumption is valid (Sheng, 2025). The modal density over the target frequency range is further validated against modal analysis results obtained from NASTRAN. Fig. 7 gives the modal density results of the proposed method and NASTRAN, which shows that the proposed method achieves excellent agreement with NASTRAN across the entire frequency range, confirming its accuracy for modal density calculation. Table 2

presents the number of modes at each center frequency as computed by the proposed method. A minimum of five modes per frequency band is commonly adopted as a practical criterion for statistical sufficiency in SEA, especially to ensure stable estimates of coupling loss factors. Moreover, the mid-frequency range has been associated with frequency bands containing more than five modes per one-third-octave band (Filippoupolitis and Hopkins, 2023), while higher modal counts together with sufficient modal overlap further improve the stability of frequency-averaged quantities (Winter, 2018). The results show that all bands at and above 630 Hz satisfy the statistical sufficiency criterion. In this example, the frequency range $[630,\ 2500]$ Hz is used as the effective analysis frequency band for VSEA.

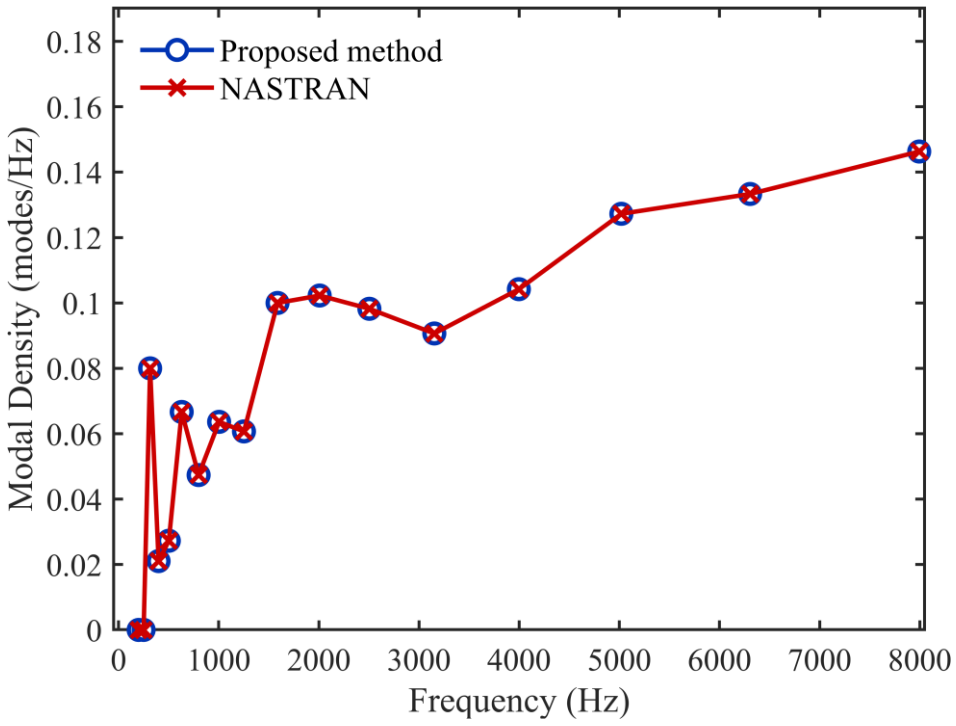


Fig. 7 Comparison of modal density results between the proposed method and NASTRAN.

Table 2 Number of modes in 1/3-octave bands obtained by the proposed method

1/3-octave band center frequency (Hz)	Lower band-edge frequency (Hz)	Upper band-edge frequency (Hz)	Number of modes in band
200	180	224	0
250	224	280	0
315	280	355	6
400	355	450	2
500	450	560	3
630	560	710	10
800	710	900	9
1000	900	1120	14
1250	1120	1400	17
1600	1400	1800	40
2000	1800	2240	45
2500	2240	2800	55
3150	2800	3550	68
4000	3550	4500	99
5000	4500	5600	140
6300	5600	7100	200
8000	7100	9000	278

Free modal analysis is performed to extract the natural frequencies and corresponding mode shapes of the structure, which are required for the subsequent VSEA. A total of 217 system modes (excluding rigid-body modes) up to 3000 Hz are extracted using both the proposed method and NASTRAN. Eleven representative natural frequencies are selected at uniform intervals, and the computed values along with relative errors are listed in Table 3. The results show excellent agreement between the two methods, with all relative errors in natural frequencies below 0.01%. As shown in Fig. 8, representative mode shapes across the frequency range are selected, and their contours with MAC values are presented. All MAC values are close to 1, indicating excellent agreement between the proposed method and NASTRAN results.

Table 3 Natural frequency (Hz) obtained from the proposed method and NASTRAN.

Order	NASTRAN	Proposed method	Relative error (%)
7	118.927273	118.926966	0.0025
27	632.844432	632.844684	0.0045
47	1031.80541	1031.80496	0.0043
67	1341.54691	1341.54547	0.0011
87	1536.11649	1536.11569	0.0052
107	1720.39692	1720.39441	0.0015
127	1966.98385	1966.98470	0.0051
147	2175.17286	2175.17092	0.0088
167	2361.33379	2361.33198	0.0076
187	2584.34639	2584.34461	0.0069
223	2991.34248	2991.34157	0.0030

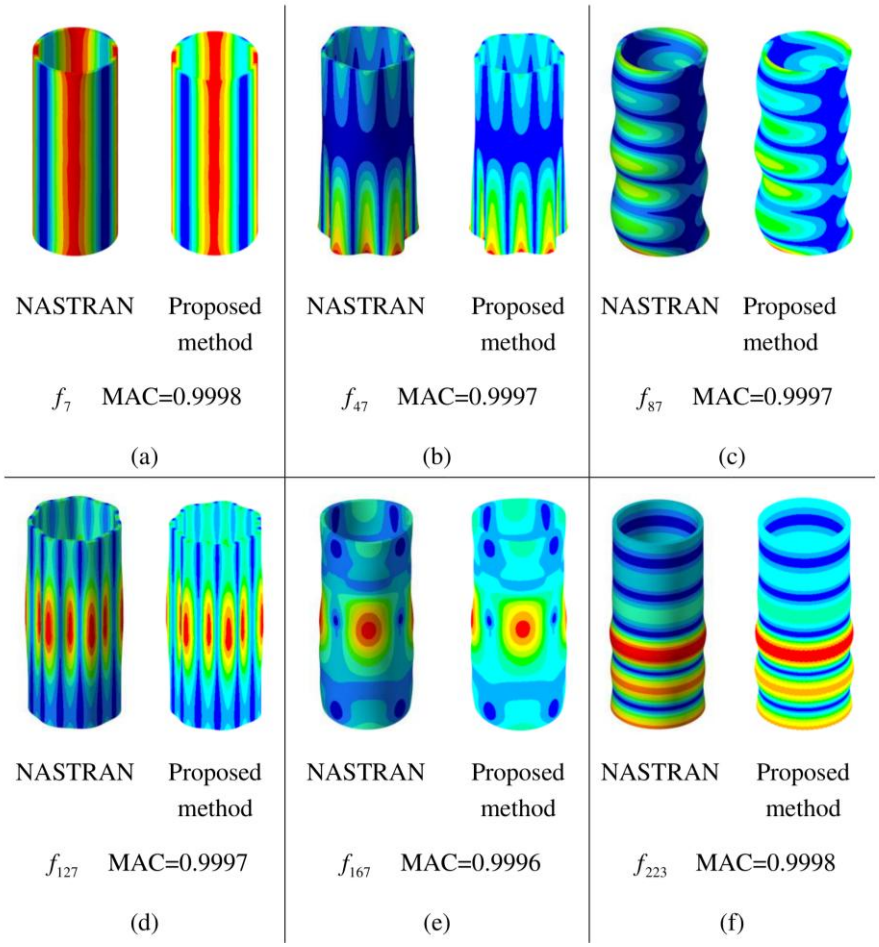


Fig. 8 Mode shapes obtained from the proposed method and NASTRAN and corresponding MAC values for the composite cylindrical shell.

VSEA is conducted based on the global modal analysis and the effective frequency band $[630,\ 2500]$ Hz identified from the modal density calculation. Following the procedure outlined in Section 2, the PIM is applied using the previously extracted modal data to compute the internal loss factors and coupling loss factors of the cylindrical shell. An input power of 10 W is applied to Subsystem 1, and a structural damping model with a uniform loss factor of 0.02 is adopted. The energy responses of all subsystems are computed across the same set of one-third-octave bands. For validation, an identical VSEA simulation is carried out using ACTRAN under the same conditions. As shown in Fig. 9, the subsystem energy results calculated by the proposed method agree closely with the ACTRAN results, with a maximum relative error below 1%, demonstrating the accuracy of the proposed method.

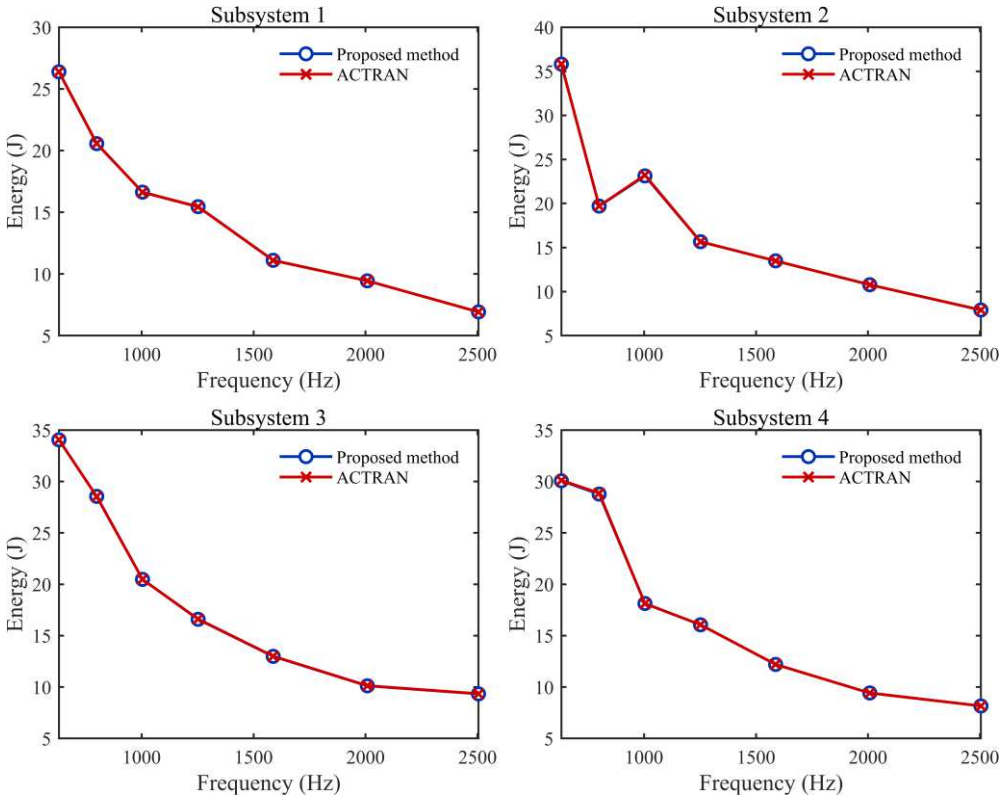


Fig. 9 Comparison of subsystem energy obtained from the proposed method and NASTRAN.

Overall computational efficiency is summarized as follows: for modal density calculation up to 8000 Hz and for modal analysis up to 3000 Hz, the proposed method requires 25 s and 255 s, respectively, while NASTRAN requires 6627 s to complete the above two computations. The total time of the proposed method is about 22 times faster than NASTRAN. In addition, the VSEA simulation is finished in 300 s and 330 s required by proposed method and ACTRAN, respectively. These results confirm that the proposed method achieves high efficiency for both modal density calculation and modal analysis of complex periodic cylindrical structures.

5.2 Example 2: Aluminum Honeycomb Cylindrical Shell

As shown in Fig. 10 (a), an aluminum honeycomb cylindrical shell is selected as a second numerical example to further demonstrate the applicability of the proposed method to complex sandwich periodic structures. The structure has a height of 2.56 m, a radius of 0.3 m, and a total thickness of 0.03 m, consisting of two outer aluminum alloy face sheets with a thickness of 3 mm each bonded to a central aluminum honeycomb core with a thickness of 6 mm, in which the honeycomb cells are regular hexagons with a side length of 12 mm. The face sheets and honeycomb core are both made of aluminum, with density $\rho_s = 2700\ \mathrm{kg/m^3}$, Young's modulus $E = 0.7\times10^{11}\ \mathrm{N/m^2}$, Poisson's ratio $\mu = 0.33$. The corresponding finite element model contains about 470,000 elements and 270,000 nodes, and the minimum shell element size is 0.01 m. Based on the structural configuration of the sandwich construction, the aluminum honeycomb cylindrical shell is subdivided into three subsystems according to the two face sheets and the honeycomb core, as illustrated in

Fig. 10 (b).

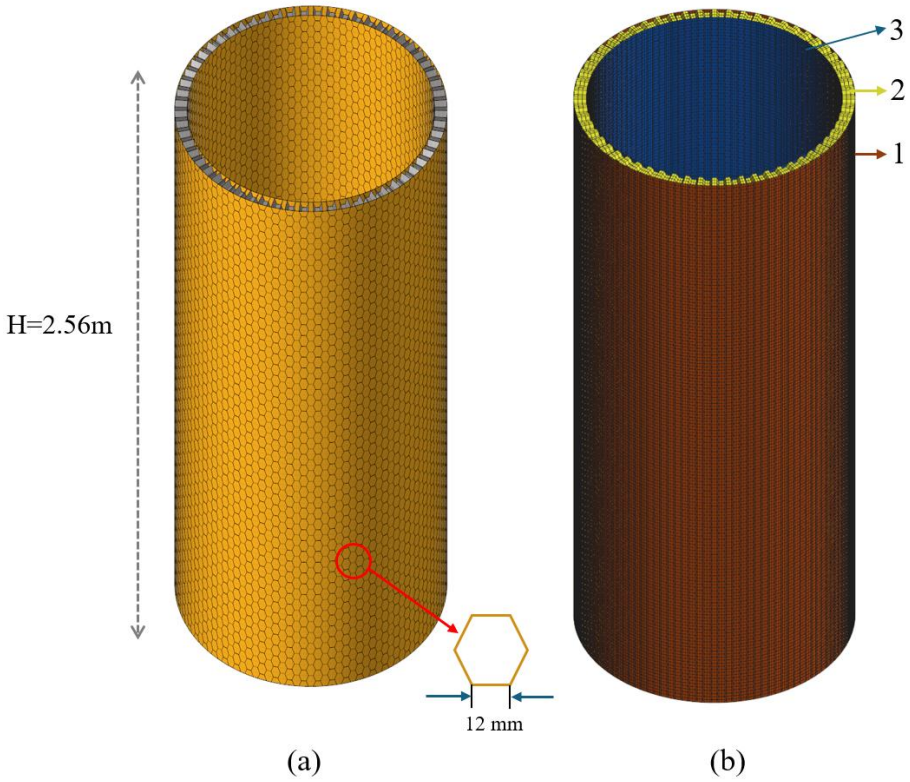


Fig. 10 Aluminum honeycomb cylindrical shell model.

The modal density of the structure is first calculated up to 8 kHz within standard one-third-octave bands. Fig. 11 compares the modal density curves obtained by the proposed method and NASTRAN, showing excellent agreement across the entire frequency range. Table 4 lists the number of modes in each frequency band. Following the same criterion as in Example 1, the results show that the frequency range $[630,\ 2500]$ Hz can be identified as the effective analysis frequency band for VSEA of the aluminum honeycomb cylindrical shell.

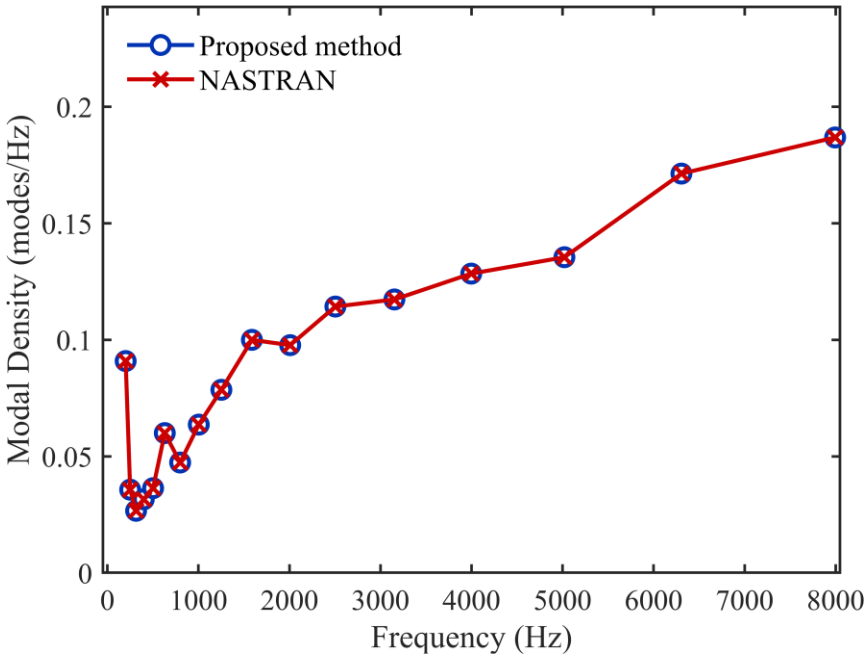


Fig. 11 Comparison of modal density results between the proposed method and NASTRAN.

Table 4 Number of modes in 1/3-octave bands obtained by the proposed method.

1/3-octave band center frequency (Hz)	Lower band-edge frequency (Hz)	Upper band-edge frequency (Hz)	Number of modes in band
200	180	224	4
250	224	280	2
315	280	355	2
400	355	450	3
500	450	560	4
630	560	710	9
800	710	900	9
1000	900	1120	14
1250	1120	1400	22
1600	1400	1800	40
2000	1800	2240	43
2500	2240	2800	64
3150	2800	3550	88
4000	3550	4500	122
5000	4500	5600	149
6300	5600	7100	257
8000	7100	9000	355

The free modal analysis is carried out to extract the natural frequencies and corresponding mode shapes. Using both the proposed method and NASTRAN, a total of 248 structural modes (excluding rigid-body modes) up to 3000 Hz are extracted. Eleven representative natural frequencies are selected at uniform intervals, and the corresponding results and relative errors are listed in Table 5. All relative errors are below 0.01%, indicating excellent agreement between the two methods. As shown in Fig. 12, the representative mode shapes over the considered frequency range yield MAC values close to 1, confirming near-perfect correlation and further validating the accuracy of the proposed method in calculating mode shapes.

Table 5 Natural frequency (Hz) and corresponding relative error obtained from the proposed method and NASTRAN.

Order	NASTRAN	Proposed method	Relative Error (%)
7	189.768119	189.768279	0.0084
37	831.481387	831.480825	0.0068
57	1146.96213	1146.96302	0.0078
87	1525.60751	1525.60943	0.0126
107	1661.51186	1661.51267	0.0048
127	1872.68899	1872.68828	0.0037
147	2042.35798	2042.35791	0.0034
167	2232.38636	2232.38509	0.0057
187	2395.90961	2395.90795	0.0069
217	2663.58989	2663.59130	0.0053
248	2975.89681	2975.89595	0.0029

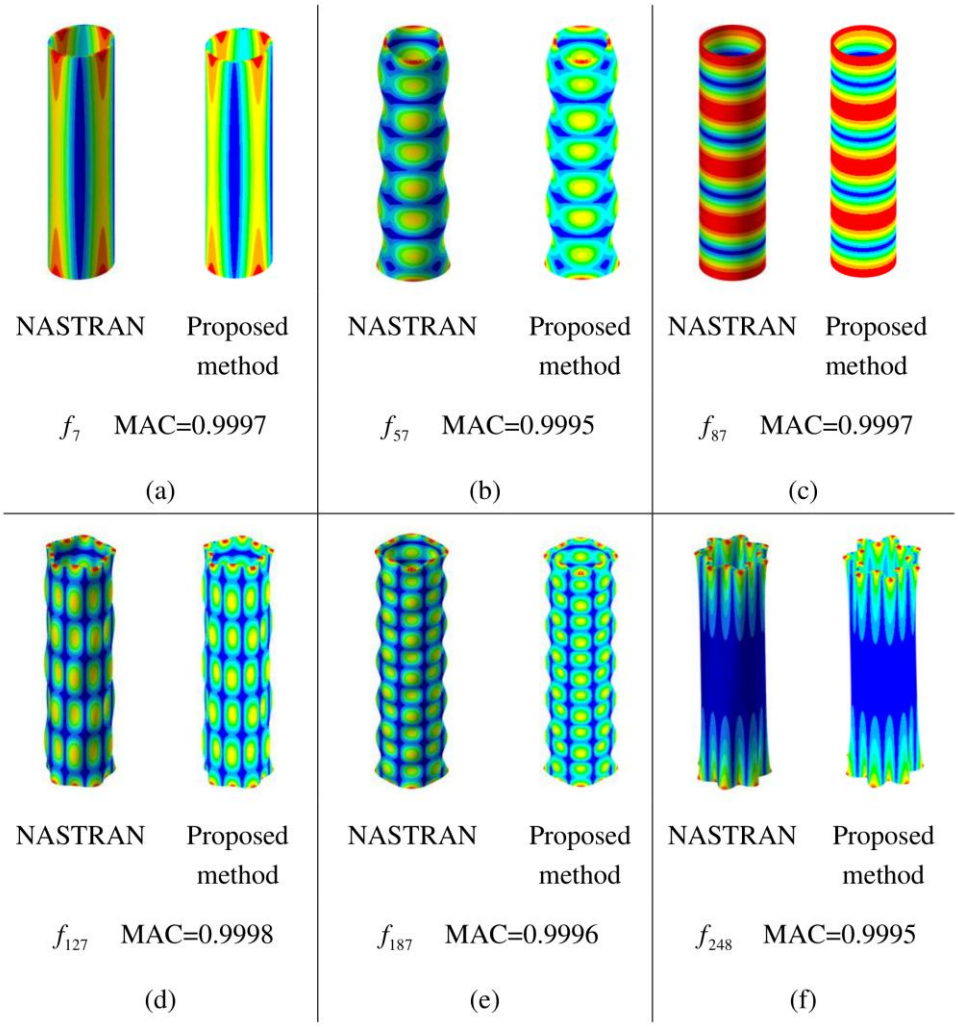


Fig. 12 Mode shapes obtained from the proposed method and NASTRAN and corresponding MAC values for the aluminum honeycomb cylindrical shell.

The PIM is applied to compute the internal loss factors and coupling loss factors of the shell, followed by VSEA over the identified frequency band $[630,\ 2500]$ Hz. An input power of 10 W is applied to Subsystem 1, and a uniform structural damping model with a loss factor of 0.02 is adopted. The steady-state energy responses of all subsystems are computed across the same one-third-octave bands. For validation, an equivalent VSEA simulation is performed using ACTRAN under identical modeling

and analysis conditions. As shown in Fig. 14, the calculated subsystem energy results from the proposed method closely match ACTRAN results, with a maximum relative error below 1%, demonstrating the high accuracy of the proposed method.

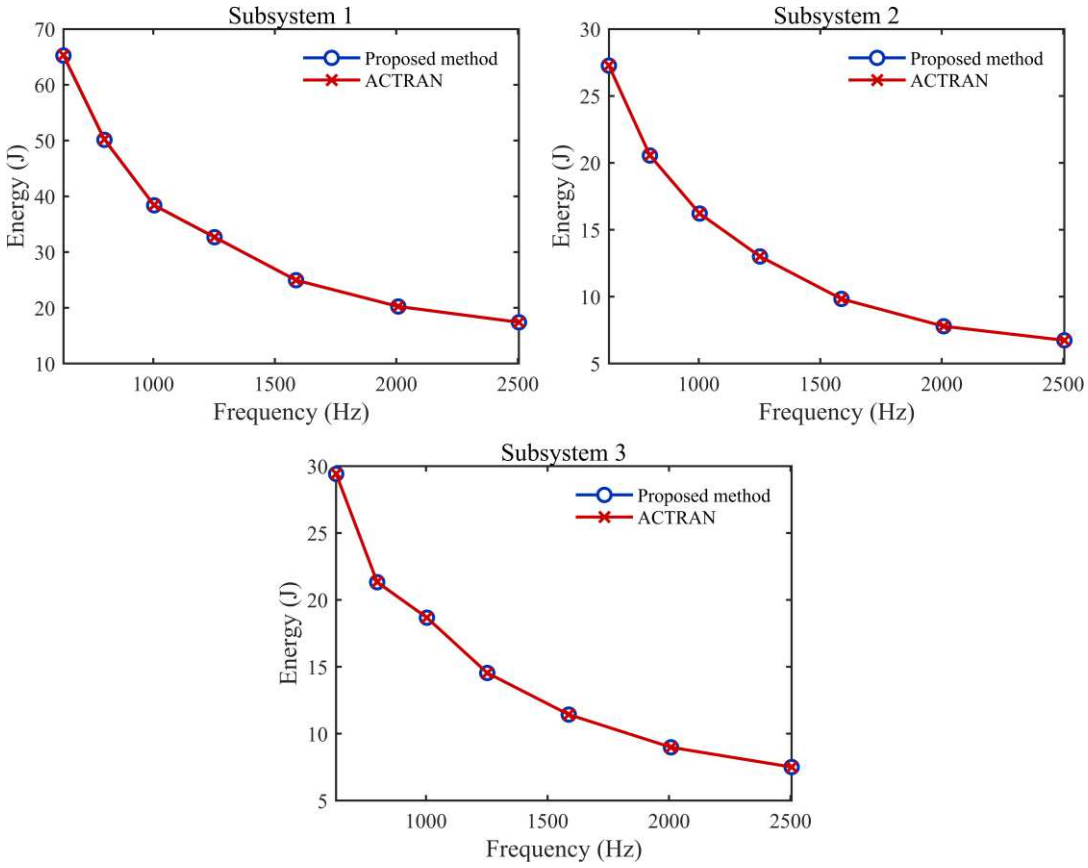


Fig. 14 Comparison of subsystems energy obtained from the proposed method and NASTRAN.

The overall computational efficiency is summarized as follows: for modal density calculation up to 8000 Hz and modal analysis up to 3000 Hz, the proposed method requires 55 s and 240 s, respectively, while NASTRAN requires 10,037 s to complete the above two computations. The total time of the proposed method is about 33 times faster than NASTRAN. For the VSEA simulation, the proposed method requires 480 s, ACTRAN requires 530 s. Overall, these results demonstrate that the proposed method

is highly efficient for both modal density calculation and modal analysis of complex periodic cylindrical structures.

6. Conclusion

In this paper, an efficient VSEA method for cylindrical periodic structures is proposed to improve the computational efficiency of mid-to-high frequency vibration analysis. Based on group theory, the global structure is circumferentially decoupled. Then, the W-W algorithm combined with a bisection strategy is employed to efficiently compute modal density, natural frequencies and mode shapes required for SEA parameter identification. Based on these results, the PIM is applied to determine the internal and coupling loss factors and to calculate subsystem energy responses. Numerical examples demonstrate that the proposed method achieves excellent agreement with commercial software. An overall computational speedup of approximately 20-30 times is obtained compared with NASTRAN for modal density calculation and modal analysis of complex periodic cylindrical structures, while the VSEA simulation time remains comparable to that of ACTRAN.

Appendix A

According to the node grouping strategy, matrices $\mathbf{K}_I^0$, $\mathbf{K}_{II}^0$ and $\mathbf{K}_{III}^0$ exhibit structural properties characteristic of a one-dimensional structure. Based on the continuity of shared nodes between adjacent unit cells, the matrices $\mathbf{K}_I^0$, $\mathbf{K}_{II}^0$ and

$\mathbf{K}_{III}^{0}$ can be formulated as shown in Eq. (19), where the components are defined as follows:

$$\mathbf{K}_{I}^{1}=\begin{bmatrix}\mathbf{K}_{aa} & \mathbf{K}_{ab} & \mathbf{K}_{ac} & \mathbf{K}_{ai}\\ \mathbf{K}_{ba} & \mathbf{K}_{bb} & \mathbf{K}_{bc} & \mathbf{K}_{bi}\\ \mathbf{K}_{ca} & \mathbf{K}_{cb} & \mathbf{K}_{cc} & \mathbf{K}_{ci}\\ \mathbf{K}_{ia} & \mathbf{K}_{ib} & \mathbf{K}_{ic} & \mathbf{K}_{ii}\end{bmatrix},\ \mathbf{K}_{I}^{5}=\begin{bmatrix}\mathbf{K}_{dd} & \mathbf{K}_{de}\\ \mathbf{K}_{ed} & \mathbf{K}_{ee}\end{bmatrix}$$

$$\mathbf{K}_{I}^{2}=\begin{bmatrix}\mathbf{K}_{dd} & \mathbf{K}_{de} & \mathbf{0} & \mathbf{0}\\ \mathbf{K}_{ed} & \mathbf{K}_{ee} & \mathbf{0} & \mathbf{0}\\ \mathbf{0} & \mathbf{0} & \mathbf{0} & \mathbf{0}\\ \mathbf{0} & \mathbf{0} & \mathbf{0} & \mathbf{0}\end{bmatrix},\ \mathbf{K}_{I}^{3}=\left(\mathbf{K}_{I}^{4}\right)^{\mathrm{T}}=\begin{bmatrix}\mathbf{K}_{ad} & \mathbf{K}_{ae} & \mathbf{0} & \mathbf{0}\\ \mathbf{K}_{bd} & \mathbf{K}_{be} & \mathbf{0} & \mathbf{0}\\ \mathbf{K}_{cd} & \mathbf{K}_{ce} & \mathbf{0} & \mathbf{0}\\ \mathbf{K}_{id} & \mathbf{K}_{ie} & \mathbf{0} & \mathbf{0}\end{bmatrix} \tag{A.1}$$

$$\mathbf{K}_{I}^{6}=\left(\mathbf{K}_{I}^{7}\right)^{\mathrm{T}}=\begin{bmatrix}\mathbf{K}_{ad} & \mathbf{K}_{ae}\\ \mathbf{K}_{bd} & \mathbf{K}_{be}\\ \mathbf{K}_{cd} & \mathbf{K}_{ce}\\ \mathbf{K}_{id} & \mathbf{K}_{ie}\end{bmatrix}$$

$$\mathbf{K}_{II}^{1}=\begin{bmatrix}\mathbf{0} & \mathbf{0} & \mathbf{0} & \mathbf{0}\\ \mathbf{0} & \mathbf{K}_{ff} & \mathbf{K}_{fg} & \mathbf{0}\\ \mathbf{0} & \mathbf{K}_{gf} & \mathbf{K}_{gg} & \mathbf{0}\\ \mathbf{0} & \mathbf{0} & \mathbf{0} & \mathbf{0}\end{bmatrix}\mathbf{0},\ \mathbf{K}_{II}^{3}=\left(\mathbf{K}_{II}^{4}\right)^{\mathrm{T}}=\begin{bmatrix}\mathbf{0} & \mathbf{0} & \mathbf{0} & \mathbf{0}\\ \mathbf{0} & \mathbf{K}_{fh} & \mathbf{0} & \mathbf{0}\\ \mathbf{0} & \mathbf{K}_{gh} & \mathbf{0} & \mathbf{0}\\ \mathbf{0} & \mathbf{0} & \mathbf{0} & \mathbf{0}\end{bmatrix}$$

$$\mathbf{K}_{II}^{2}=\begin{bmatrix}\mathbf{0} & \mathbf{0} & \mathbf{0} & \mathbf{0}\\ \mathbf{0} & \mathbf{K}_{hh} & \mathbf{0} & \mathbf{0}\\ \mathbf{0} & \mathbf{0} & \mathbf{0} & \mathbf{0}\\ \mathbf{0} & \mathbf{0} & \mathbf{0} & \mathbf{0}\end{bmatrix},\ \mathbf{K}_{II}^{5}=\begin{bmatrix}\mathbf{0} & \mathbf{0}\\ \mathbf{0} & \mathbf{K}_{hh}\end{bmatrix},\ \mathbf{K}_{II}^{6}=\left(\mathbf{K}_{II}^{7}\right)^{\mathrm{T}}=\begin{bmatrix}\mathbf{0} & \mathbf{0}\\ \mathbf{0} & \mathbf{K}_{fh}\\ \mathbf{0} & \mathbf{K}_{gh}\\ \mathbf{0} & \mathbf{0}\end{bmatrix} \tag{A.2}$$

$$\mathbf{K}_{III}^{1}=\begin{bmatrix}0 & \mathbf{K}_{af} & \mathbf{K}_{ag} & 0\\ 0 & \mathbf{K}_{bf} & \mathbf{K}_{bg} & 0\\ 0 & \mathbf{K}_{cf} & \mathbf{K}_{cg} & 0\\ 0 & \mathbf{K}_{lf} & \mathbf{K}_{lg} & 0\end{bmatrix},\ \mathbf{K}_{III}^{2}=\begin{bmatrix}0 & \mathbf{K}_{dh} & 0 & 0\\ 0 & \mathbf{K}_{eh} & 0 & 0\\ 0 & 0 & 0 & 0\\ 0 & 0 & 0 & 0\end{bmatrix}$$

$$\mathbf{K}_{III}^{3}=\begin{bmatrix}0 & \mathbf{K}_{ah} & 0 & 0\\ 0 & \mathbf{K}_{bh} & 0 & 0\\ 0 & \mathbf{K}_{ch} & 0 & 0\\ 0 & \mathbf{K}_{lh} & 0 & 0\end{bmatrix},\ \mathbf{K}_{III}^{4}=\begin{bmatrix}0 & \mathbf{K}_{df} & \mathbf{K}_{dg} & 0\\ 0 & \mathbf{K}_{ef} & \mathbf{K}_{eg} & 0\\ 0 & 0 & 0 & 0\\ 0 & 0 & 0 & 0\end{bmatrix} \tag{A.3}$$

$$\mathbf{K}_{III}^{5}=\begin{bmatrix}0 & \mathbf{K}_{dh}\\ 0 & \mathbf{K}_{eh}\end{bmatrix},\ \mathbf{K}_{III}^{6}=\begin{bmatrix}0 & \mathbf{K}_{ah}\\ 0 & \mathbf{K}_{bh}\\ 0 & \mathbf{K}_{ch}\\ 0 & \mathbf{K}_{lh}\end{bmatrix},\ \mathbf{K}_{III}^{7}=\begin{bmatrix}0 & \mathbf{K}_{df} & \mathbf{K}_{dg} & 0\\ 0 & \mathbf{K}_{ef} & \mathbf{K}_{eg} & 0\end{bmatrix}$$

Declaration of competing interest

The authors declare that they have no known competing financial interests or personal relationships that could have appeared to influence the work reported in this paper.

Acknowledgment

The authors are grateful for the National Natural Science Foundation of China (No. 12472196), the financial support of the Research Fund of National Key Laboratory of Aerospace Physics in Fluids (Grant No. 2025-APF-KFMS-19) and the National Key R&D Program of China (No. 2022YFB4201200) and the development and application project of ship CAE software. This work is supported by other funding.

Data availability

No data was used for the research described in the article.

References

Andrade, L., Langley, R.S., Butlin, T., 2022. Extension of a hybrid FE-SEA approach for vibro-acoustic analysis with prescribed displacements. Journal of Sound and Vibration 529, 116912.

Ashari, A.K., Stephen, N.G., 2026. Static and dynamic analysis of repetitive structures with intermediate supports using wave transfer matrix method. European Journal of Mechanics - A/Solids 116, 105936.

Avetisyan, A., Ghazaryan, K., Marzocca, P., 2026. Flexural vibration analysis of a beam partially covered by a piezoelectric patch and resting on periodic supports. European Journal of Mechanics - A/Solids 116, 105942.

Banerjee, J.R., Williams, F.W., 1996. Free vibration of two-dimensional frameworks by using the Wittrick–Williams algorithm. International Journal of Solids and Structures 33(24), 3549-3563.

Bies, D., Hamid, S., 1980. In situ determination of loss and coupling loss factors by the power injection method. Journal of Sound and Vibration 70(2), 187-204.

Borello, G., 2010. Virtual SEA analysis of a warship classification. In: Proc. Congrès Français d'Acoustique. (Conference paper).

Bouhaj, M., von Estorff, O., Peiffer, A., 2017. An approach for the assessment of the statistical aspects of the SEA coupling loss factors and the vibrational energy transmission in complex aircraft structures: Experimental investigation and methods benchmark. Journal of Sound and Vibration 403, 152-172.

Bremner, P., Bloor, M., Wilby, J.F., 2002. Recent developments in statistical energy analysis for aircraft interior noise. Journal of the Acoustical Society of America 112(5), 2348-2356.

Chen, Y., Sareh, P., Feng, J., Sun, Q., 2017. A computational method for automated detection of engineering structures with cyclic symmetries. Computers & Structures 191, 153-164.

Duhamel, D., Mencik, J.-M., 2022. Time response analysis of periodic structures via wave-based absorbing boundary conditions. European Journal of Mechanics -

A/Solids 91, 104418.

Fahy, F., Ruivo, H., 1997. Determination of statistical energy analysis loss factors by means of an input power modulation technique. Journal of Sound and Vibration 203(5), 763-779.

Fazail, M.N.B., Chazot, J.-D., Lefebvre, G., Atalla, N., 2023. Damping loss factor characterization of complex structures using a Green's function-based model. Journal of Sound and Vibration 552, 117642.

Fazzolari, F.A., Tan, P., 2020. A hybrid finite element-statistical energy analysis approach for the dynamic response of built-up systems with nonlinear joints. Journal of Sound and Vibration 489, 115696.

Filippoupolitis, M., Hopkins, C., 2023. Vibration transmission across seismically damaged beam-to-column junctions of reinforced concrete using statistical energy analysis. Vibration 6(1), 149-164.

Gagliardini, L., Houillon, L., Petrinelli, L., Borello, G., 2003. Virtual SEA: Mid-Frequency Structure-Borne Noise Modeling Based on Finite Element Analysis. SAE Technical Paper 2003-01-1555.

Guo, W., Li, J., Luo, W., Yang, J., Zhu, X., Yan, J., 2025. A new method for solving parameter mutation analysis in periodic structure bandgap calculation. European Journal of Mechanics - A/Solids 111, 105572.

Harth, P., Michelberger, P., 2016. Determination of loads in quasi-symmetric structure with symmetry components. Engineering Structures 123, 395-407.

Hexagon, 2024. ACTRAN 2024.2 User's Guide - Volume 1: Installation, Operations,

Theory and Utilities. Hexagon.

Hynnä, P., Klinge, P., Vuoksinen, J., 1995. Prediction of structure-borne sound transmission in large welded ship structures using statistical energy analysis. Journal of Sound and Vibration 180(4), 583-607.

Jeong, W., Park, K., 2009. Application of Virtual SEA for the prediction of acoustic performance of cockpit. SAE Technical Paper 2009-01-0767.

Kangwai, R.D., Guest, S.D., 2000. Detecting symmetry in finite element models. International Journal of Solids and Structures 37(5), 1525-1548.

Kangwai, R.D., Guest, S.D., Pellegrino, S., 1999. An introduction to the analysis of symmetric structures. Computers & Structures 71(6), 671-688.

Langley, R.S., Heron, K.H., 1990. Elastic wave propagation in periodic structures: The Wittrick–Williams algorithm and its application to waveguides. International Journal of Solids and Structures 26(7), 819-835.

Lee, H.R., Kim, H.Y., Jeon, J.H., Kang, Y.J., 2019. Application of global sensitivity analysis to statistical energy analysis: Vehicle model development and transmission path contribution. Applied Acoustics 146, 368-389.

Liang, X., Gao, Q., Yao, W., 2018. An efficient method for the dynamic responses of periodic structures based on the physical features of the structure and group theory. International Journal of Mechanical Sciences 141, 461-478.

Lyon, R., 1974. Statistical energy analysis of dynamical systems: theory and applications. MIT Press, Cambridge, MA.

Lyon, R.H., Maidanik, G., 1962. Power flow between linearly coupled oscillators.

Journal of the Acoustical Society of America 34, 623-639.

Mace, B., Shorter, P., 2000. Energy flow models from finite element analysis. Journal of Sound and Vibration 233, 369-389.

Mace, B.R., 1995. Statistical energy analysis: Hamilton's principle and system representation. International Journal of Solids and Structures 32(7), 1067–1084.

Maksimov, D.N., Tanner, G., 2011. A hybrid approach for predicting the distribution of vibro-acoustic energy in complex built-up structures. Journal of the Acoustical Society of America 130(3), 1337-1347.

Marzani, A., Viola, E., 2005. Free wave propagation in periodic beam lattices by the Wittrick–Williams algorithm. International Journal of Solids and Structures 42(4), 1161-1183.

Maxit, L., Guyader, J.-L., 2001. Estimation of SEA coupling loss factors using a dual formulation and FEM modal information. Part I: Theory. Journal of Sound and Vibration 239(5), 907-930.

Peeters, M.F., Tromp, P.J., 1985. Dynamic analysis of cyclic symmetric structures by block-diagonalization. International Journal of Solids and Structures 21(12), 1201-1215.

Poblet-Puig, J., 2021. Estimation of the coupling loss factors of structural junctions with in-plane waves by means of the inverse statistical energy analysis problem. Journal of Sound and Vibration 493, 115850.

Qu, Y., Chen, Y., Long, X., Hua, H., Meng, G., 2013. A modified variational approach for vibration analysis of ring-stiffened conical–cylindrical shell combinations.

European Journal of Mechanics - A/Solids 37, 200-215.

Sheng, M., 2025. Modal density evaluation of a fluid-loaded free-damping stiffened plate. Journal of Marine Science and Engineering 13(8), 1551.

Sipos, D., Treszkai, M.F., Feszty, D., 2022. Validation of finite element connection modeling by comparison of experimental and virtual power injection methods. Journal of Vibroengineering 25(1), 209-225.

Takhchi, J., Ouisse, M., Sadoulet-Reboul, E., Bouhaddi, N., Gagliardini, L., Bornet, F., Gavric, L., Lakrad, F., 2024. A method to investigate mid and high-frequency vibration energy transfer paths using the irrotational intensity. Journal of Sound and Vibration 572, 118160.

Winter, C.K., 2018. Frequency dependent modeling for the prediction of the sound transmission in timber constructions (PhD thesis). Technical University of Munich, Germany.

Wittrick, W.H., Williams, F.W., 1971. A general algorithm for computing natural frequencies of elastic structures. Quarterly Journal of Mechanics and Applied Mathematics 24(3), 263-284.

Yang, Z., Luo, W., You, C., He, H., Chen, S., Zhang, P., Guo, W., 2026. Lightweight design for low-frequency vibration reduction in periodic floating slab tracks based on the wave singular value decomposition method. European Journal of Mechanics - A/Solids 119, 106164.

Yin, J., Hopkins, C., 2013. Prediction of high-frequency vibration transmission across coupled, periodic ribbed plates by incorporating tunneling mechanisms. Journal of

the Acoustical Society of America 133(4), 2069-2081.

Zhang, S., Sheng, X., Yang, S., Chen, Z., 2020. Improving the double-exponential windowing method to identify modal frequencies and damping ratios of dynamically large structures. Journal of Sound and Vibration 476, 115314.

Zhu, G., Maxit, L., Totaro, N., Le Bot, A., 2022. A hybrid modal/statistical formulation for predicting the energy response of vibroacoustic systems in the mid frequency range. Journal of Sound and Vibration 538, 117221.

Zingoni, A., 1997. Vibration analysis of repetitive structures using block–circulant matrices. International Journal of Solids and Structures 34(16), 2025-2041.

Zingoni, A., 2015. On the use of group-theoretic and block-circulant matrix methods for the vibration analysis of repetitive structures. International Journal of Solids and Structures 56-57, 170-181.